Stability, Properties, and Electronic g Tensors of the H_2COH Radical

Pablo J. Bruna and Friedrich Grein*

Department of Chemistry, University of New Brunswick, Fredericton, NB E3B 6E2, Canada

Received: September 18, 1997; In Final Form: January 19, 1998

For the H_2COH radical, properties such as geometries, frequencies, electric and magnetic dipole moments, electronic and ionization spectra, etc., were investigated at the ab initio level (second-order Møeller−Plesset and multireference configuration interaction (MRD-CI) methods). At equilibrium, H_2COH ($\sigma^2\pi^2n^2\pi^*$) is of C_1 symmetry. The inversion and rotation conformations are about 1 and 5 kcal/mol less stable. The MRD-CI vertical ionization potentials (eV) lie at 7.89 ($\pi^* \rightarrow \infty$) and 12.91 ($n \rightarrow \infty$, into $1^3A''$ of the cation). The $\pi^* \rightarrow 3s$ state (adiabatically at $T_e \approx 3.23$ eV, calculated) is placed about 1 eV lower than previously assumed. Experimental T_0's of 4.34 and 5.09 eV are respectively reassigned to $\pi^* \rightarrow 3p_z$ and $\pi^* \rightarrow 3p_x$ (perpendicular and parallel bands relative to the CO bond). At the equilibrium geometry, the valence states lie at 6.46 ($n \rightarrow \pi^*$), 7.30 ($\pi \rightarrow \pi^*$), and 8.40 eV ($\sigma \rightarrow \pi^*$); i.e., the latter lies in the ionization continuum. The direction of the electric dipole moment of H_2COH is mainly governed by the OH bond. The electron-spin magnetic moment (g factor) was evaluated via a perturbative approach complete to second order, using a Breit−Pauli Hamiltonian. The largest second-order contributions to Δg are due to $\sigma \rightarrow \pi^*$ and $n \rightarrow \pi^*$. At the ROHF level, $\Delta g_{av} = g_{av} - g_e$ is ∼500 ppm for both the equilibrium and inversion conformations and near 300 ppm for the rotation geometry. Correlated values are estimated to be ∼150 ppm higher. Experimental studies for H_2COH in solution find $\Delta g_{av} \approx 1000$ ppm.

Introduction

The hydroxymethyl radical (H_2COH), which plays an important role in the combustion of hydrocarbon fuels, atmospheric pollution chemistry, surface science, and interstellar chemistry, has been the subject of numerous theoretical and experimental investigations. See Johnson and Hudgens's paper (JH)[1] for a detailed bibliography covering more than 100 references.

To date, the most extensive theoretical works on H_2COH are due to Johnson and Hudgens,[1] Saebo, Radom and Schaefer (SRS),[2] and Bauschlicher and Partridge (BP),[3] who analyzed in detail the ground-state potential energy surface (PES) near equilibrium. Relevant features of this surface are summarized below.

Formally, H_2COH can be obtained via hydrogenation of formaldehyde. Placing H_2CO (C_{2v}) in the *yz* plane and the CO bond collinear to the *z* axis, one can first consider an H atom approaching H_2CO along the *z* axis toward O to form H_2COH with C_{2v} symmetry. Although this conformation is energetically unstable, it serves as a good reference frame to analyze several properties of H_2COH. Starting from H_2COH (C_{2v}) and by bending the COH group into either the *yz* or the *xz* plane, two different C_s structures can be generated, the so-called *inversion* (H_2COH(i)) and *rotation* (H_2COH(r)) conformations, respectively. Figure 1 displays the corresponding structures. For convenience, the C−O bond is always placed along the *z*-axis, and therefore the coordinate system for the two C_s structures is nonstandard.

For H_2COH(i) with $C_s(yz)$ symmetry, all atoms lie in the molecular (symmetry) plane; the CH bond lengths are different. For the $C_s(xz)$ rotation structure, the COH group lies in the symmetry plane, and the H_2CO moiety is pyramidal (with equal CH bonds). Earlier theoretical studies,[4,5] none of which calculated vibrational frequencies to check for local instabilities, assumed that H_2COH has the inversion, the rotation, or a hybrid structure. However, in 1983, Saebo et al. found that both C_s conformations actually correspond to saddle points, with one imaginary frequency each. The equilibrium structure of H_2COH, hereafter designated as H_2COH(eq), is totally nonsymmetrical (C_1), with the COH group lying in neither the *yz* nor *xz* planes, but between; the H_2CO moiety is pyramidal as in H_2COH(r), but with nonequal CH bonds. According to theoretical studies, the height of the CH_2 inversion barrier is 0.45 [1] and 0.92 kcal/mol,[2] with the OH rotation barrier being larger (4.70 [1,3] and 3.98 kcal/mol [2]).

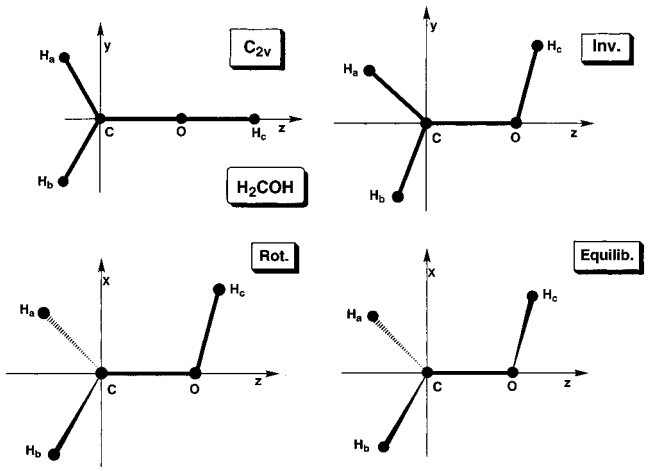

Figure 1. H_2COH conformations studied in this work. The conformations of the X^1A' and $1^3A''$ states of H_2COH^+ are similar to those of H_2COH(inv), and H_2COH(rot), respectively.

Regarding the electronic structure, the C_{2v} radical has an X $^2B_1$ ground state, with the unpaired electron in the π^* MO oriented perpendicular to the molecular plane. For the inversion

* Corresponding author: (e-mail) FRITZ@UNB.CA.

S1089-5639(97)03066-1 CCC: $15.00
Published on Web 04/11/1998

conformation, where the mixing a_1/b_2 (σ/n) is possible, the ground state is X $^2A''$, with the SOMO also being a pure π^* species; here, the OH bond orbital consists of 1s(H) and the highest-lying $\sigma(5a_1)$ and n($2b_2$) MOs of H_2CO. At the rotation geometry, where the mixing a_1/b_1 (σ/π) is allowed, the ground-state becomes X $^2A'$, with the π^* SOMO lying in the symmetry plane and the n($2b_2$) oxygen lone pair being perpendicular to it. For the C_1 equilibrium geometry, the H_2COH radical is characterized by an electronic ground state ^2A in which the mixing $a_1/b_1/b_2$ (σ/π/n) is possible. Because of the rather small inversion barrier, Johnson and Hudgens[1] concluded that H_2COH effectively belongs to the $C_s(yz)$ point group having the inversion geometry, for which the electronic ground state corresponds to X $^2A''$.

Experimental information about the structure and bonding of H_2COH has been gained by analyzing the vibrational,[1,6] electronic,[1,7,8] photoionization,[9,10] and electron spin resonance (ESR)[11−14] spectra. The electronic spectrum, measured up to 6.0 eV, consists of Rydberg transitions only, assumed to be of type $\pi^* \rightarrow$ 3s, 3p.[7,15] The adiabatic ionization potential (IP) of H_2COH ($\pi^* \rightarrow \infty$, 7.56 eV[9]) is relatively low when compared with that of H_2CO (n $\rightarrow \infty$, 10.88 eV), reflecting the low excitation energies of the Rydberg states in the radical.

ESR studies for H_2COH in solution reported hyperfine coupling constants (hfcc) and the average electronic g factor, the latter parameterizing the electron-spin magnetic moment. Three independent experimental values of $\Delta g_{av} = g_{av} - g_e$ are available, namely 1031,[11] 970 ± 30,[13] and 981 ppm,[14] the first two from measurements in aqueous and the last one in *tert*-pentyl alcohol solutions. The Δg_{av} value of H_2CO^-, a radical isoelectronic with H_2COH, is ∼500 ppm larger.[14]

Krusic et al.[12] studied the temperature dependence (from 148 to 215 K) of the β-proton hfcc and corresponding line shapes. On the basis of this information, they estimated a barrier height of ∼4.3 kcal/mol for the hindered rotation of OH about the CO bond, a value confirmed by ab initio results (see above).

In this work, we focus on the calculation of several properties of H_2COH (at equilibrium as well as at the inversion and rotation conformations) that have received little or no attention before, such as the ionization potentials for several MOs, the electronic spectrum including both Rydberg and valence states, with corresponding oscillator strengths, dipole moments (electric as well as electron-spin magnetic), etc. While **g**-tensor calculations of H_2COH were mostly performed at the ROHF level, some correlated studies have also been included, as done recently for (H_2CO^-)(Na^+) complexes.[16] Of particular interest for the **g**-tensor calculations on H_2COH are the valence excitations n $\rightarrow \pi^*$ and $\sigma \rightarrow \pi^*$, which have not yet been observed experimentally.

Methods

(1) Basis Sets and Programs Used. Standard properties (equilibrium geometries, harmonic vibrational frequencies and their absorption intensities, electric dipole moments, spin density distributions, Fermi contact term (FCT), etc.) were calculated with GAUSSIAN90.[17] Since the spin contamination is relatively minor, the unrestricted HF (UHF) procedure was found to work well for H_2COH. Geometry optimizations were carried out at the MP2(full) level using a 6-311G(d,p) basis set. Single-point calculations were also done with the expanded basis set 6-311++G(2df,2pd).

The electronic spectrum, ionization potentials and some **g** tensors were studied using a multireference CI (MRD-CI) approach, based on Table CI algorithm and extrapolation techniques.[18] For the CI expansions, the ground state (ROHF) MOs were taken, using the frozen-core approximation. The dimension of the diagonalized CI matrices lies, on average, in the range of 25 000−30 000 spin-adapted functions. The CI calculations were carried out with Huzinaga's primitive set[19] (10s6p for C and O, and 5s for H), Dunning's contraction scheme[20] (5s4p for C and O, and 3s for H), and Sadlej's polarization AOs[21] (2d/1d for C and O, and 2p/1p for H; the two most compact AOs in each case). The C center also contains 3s,3p Rydberg AOs ($\alpha_s = 0.041$, $\alpha_p = 0.027$). This basis set is called basis A. Selected calculations were also done with basis B, obtained from A by deleting the Rydberg AOs and by adding more polarization functions (4d/2d for C and O, and 4p/2p for H [21]).

(2) *g*-Factor Calculations. The electron-spin magnetic moment, $\boldsymbol{\mu}_s$, of a radical is given as $\mu_s = -\mu_B \mathbf{S}\cdot\mathbf{g}$, where μ_B is the Bohr magneton; **S**, the spin angular momentum vector; and **g**, a second rank tensor called the electronic **g** tensor.[22]

The g components can be written as $g_{ab} = g_e\delta^{ab} + \Delta g_{ab}$, where $g_e = 2.002\,319$ represents the g factor of a free electron; δ^{ab}, the Kronecker delta; and a,b is a pair of x, y, z coordinates. An increase of the magnitude of the electron spin magnetic moment (i.e., effective spin angular momentum) relative to that of a free electron, for example, corresponds to a positive Δg_{ab} value. The sign of Δg_{ab} is generally governed by the characteristics of the magnetic coupling between the electronic ground state and the excited-state manifold. For this reason, Δg data provide additional information about the structure of a radical beyond that gained from hyperfine coupling constants, which only depend on the spin density distribution of the ground state.

In this work, g shifts are calculated using a perturbative approach, complete to second order in appropriate Breit−Pauli operators. See ref 23 for a more detailed theoretical analysis of this type of calculations. In short, a given Δg_{ab} value is evaluated as the sum of *two* first-order terms and *one* second-order term. The first-order contributions (i.e., ground-state expectation values) comprise the relativistic mass correction to the spin Zeeman interaction (Δg_{RMC}) and the (one- and two-electron) spin Zeeman gauge corrections (Δg_{GC-SZ}). Some authors[24] call Δg_{GC-SZ} the *diamagnetic* terms. Generally speaking, for the compounds discussed here, the total first-order contribution is around −300 ppm for each diagonal Δg component.

The second-order part, also called the *paramagnetic* term,[24] is calculated via a sum-over-states (SOS) expansion. Each component of this expansion (called here the *magnetic coupling*) is directly proportional to the product of the spin−orbit (SO) and orbital Zeeman matrix elements (L) between the ground state and a given excited state and inversely proportional to the corresponding excitation energy. As shown in the section Electron-Spin Magnetic Moment, the SOS expansions of H_2COH are governed by the magnetic coupling with relatively few excited states of valence character, in particular $\sigma \rightarrow \pi^*$ and n $\rightarrow \pi^*$.

In C_{2v} symmetry, the **g** tensor is diagonal in the components g_{xx}, g_{yy}, and g_{zz}. In C_s, the diagonal and one pair of non diagonal g-components are nonzero (g_{yz}, g_{zy}, or g_{xz}, g_{zx}). In C_1, all nine components are nonzero.

The principal values g_1, g_2, and g_3 of the **g** tensor (i.e., the diagonal representation) can be obtained by diagonalizing the symmetric matrix $\mathbf{g}\cdot\mathbf{g}^T$, with $\mathbf{g}^T$ being the transpose matrix. The average g value, g_{av}, which is invariant upon rotation of the coordinate system, can be calculated either as $^1/_3$ ($g_{xx} + g_{yy} +$

TABLE 1: Calculated Geometries, Distances (au) and Angles in (deg), for H_2COH and H_2COH^+[a]

	CO	CH_a	CH_b	OH_c	$<H_aCO$	$<H_bCO$	$<COH_c$	$<H_aCOH_c$	$<H_bCOH_c$
H_2COH(eq) ^2A C_1	2.580	2.050	2.041	1.811	118.4	112.8	107.5	28.4	184.6
TW[b]	2.575	2.038	2.031	1.810	118.8	113.4	108.4	*c*	*c*
JH	2.567	2.035	2.028	1.811	118.8	113.5	109.4	28.4	175.4
BP	2.564	2.037	2.030	1.782	117.9	113.0	110.4	33.3	181.9
SRS									
H_2COH(i) $^2A''$ $C_s(yz)$	2.576	2.038	2.031	1.810	120.8	115.0	107.7	0.0	180.0
TW	2.563	2.026	2.020	1.780	120.5	115.5	110.5	0.0	180.0
SRS									
H_2COH(r) $^2A'$ $C_s(xz)$	2.598	2.049	2.049	1.812	117.0	117.0	107.9	103.6	−103.6
TW[d]	2.605	2.041	2.041	1.821	116.8	116.8	109.0	104.5	−104.5
GK	2.580	2.035	2.035	1.784	116.5	116.5	110.7	104.8	−104.8
SRS									
H_2COH^+ $^1A'$ $C_s(yz)$	2.359	2.061	2.056	1.853	121.8	115.5	114.2	0.0	180.0
TW	2.355	2.052	2.048	1.853	121.6	115.7	115.1	0.0	180.0
JH	2.373	2.060	2.054	1.877	121.8	115.3	115.3	0.0	180.0
CKP									
H_2COH^+ $^3A''$ $C_s(xz)$	2.518	2.101	2.101	1.872	110.8	110.8	114.0	117.0	−117.0
TW[d]									

[a] All MP2 data, except for SRS (UHF level). TW (this work): 6-311G(d,p); JH[1]: 6-311G(2df,2p); BP[3]: 6-311+G(3df,2p); SRS[2] and GK[25]: 6-31G(d,p), CKP[28]: 6-31G(d). [b] MP2(full) energy, −114.81643 au. [c] Not explicitly given. $\theta_{wag} = 27.6°$ and $\tau = -7.4°$. See ref 1 for details. [d] Out-of-plane angle: 24.8° for H_2COH and 50.0° for H_2COH^+.

g_{zz}) or $^1/_3$ ($g_1 + g_2 + g_3$). The average Δg value is defined as $\Delta g_{av} = g_{av} - g_e$.

All theoretical g factors reported here were calculated by taking the electronic charge centroid (ECC) as gauge origin.

Properties

(1) Equilibrium Geometries. Table 1 displays the optimized MP2(full)/6-311G(d,p) geometries of the ground state of H_2COH (for the equilibrium, inversion, and rotation conformations) as well as for the ground and first excited state of H_2COH^+. Prior theoretical results[1,2,3,25] are also given; experimental values are not available.

The coordinate systems were described in the Introduction. In all cases, the CO bond is collinear with the z axis.

H_2COH Radical. For the three H_2COH geometries, the average R(CO) distance is ∼2.59 au, ∼0.30 au larger than in H_2CO, but ∼0.07 b smaller than in H_3COH (methanol).[3] Thus, the CO bond of H_2COH seems to retain some double-bond character. The COH angle lies at ∼110° i.e., the OH group is almost perpendicular to the CO bond.

Compared with our MP2 results, the SCF/6-31G** data from SRS[2] are within 0.02 au for distances and ∼5° for angles (Table 1).

The present MP2(full)/6-311G(d,p) treatment places the inversion and rotation conformations (zero-point corrections not included) at 0.03 and 0.21 eV (0.7 and 4.8 kcal/mol) above H_2COH(eq), which compare well with the values reported in refs 1−3 (see Introduction).

H_2COH^+ Cation. The ground-state $^1A'(\sigma^2n^2)$ of H_2COH^+ has a planar equilibrium geometry [$C_s(yz)$], similar to that of H_2COH(i). The major difference with neutral H_2COH lies in R(CO), which is ∼0.22 au shorter in the cation due to the loss of the CO-antibonding π^* electron.

At equilibrium, the excited state $1^3A''(n\pi^*)$ of H_2COH^+ belongs to the $C_s(xz)$ point group; its geometry compares with that of H_2COH(r). This triplet state can be thought of as being generated by the following: (1) ionization $n \rightarrow \infty$ relative to H_2COH ($\sigma^2n^2\pi^*$); (2) excitation $n \rightarrow \pi^*$ relative to H_2COH^+ (σ^2n^2); (3) protonation of H_2CO in its first excited $1^3A''(n\pi^*)$ state (with a pyramidal structure). The adiabatic transition energy $^3A'' \leftarrow {}^1A'$ is 4.51 eV (MP2), ∼1 eV higher than for the corresponding transition in H_2CO.[26]

The equilibrium geometry for the singlet excited state $1^1A''(n\pi^*)$ of H_2COH^+ is expected to be close to that of $1^3A''$.

(2) Vibrational Frequencies. The harmonic vibrational frequencies and fundamental infrared absorption intensities (double-harmonic approximation) calculated at the MP2(full)/6-311G(d,p) level are summarized in Table 2. Available experimental frequencies and recent theoretical estimates[1] are also given.

As usual, ab initio calculations overestimate the measured (anharmonic) frequencies, by ∼5% at the MP2 level.

For H_2COH at equilibrium, the CO stretching frequency is ∼600 cm^{-1} smaller than in H_2CO, in line with the lengthening of the CO bond in the radical. This mode exhibits the strongest absorption intensity (104 km/mol), corroborating experimental observations.[6] Next in intensity one finds the torsion (94 km/mol) and OH stretch (61 km/mol).

The imaginary value for the CH_2 wag frequency of H_2COH-(i) and for the torsion mode of H_2COH(r) indicates that these species correspond to the transition state for CH_2 inversion and OH rotation, respectively.

There has been some controversy in the literature concerning the identity of an infrared peak at 569 cm^{-1} observed for H_2-COH formed in solid Ar by the reaction of CH_3OH with F atoms; this peak was absent, however, when the reaction was carried out using excited Ar atoms. Jacox[6] assigned this peak to the $H_2COH-HF$ complex rather than to H_2COH. In this work, we find for H_2COH(eq) a harmonic CH_2 wag frequency of 726 cm^{-1} (unscaled). Using a much larger basis set (6-311+G(3df,2p), Bauschlicher and Partridge[3] reported MP2 values of 612 (unscaled) or 578 cm^{-1} (scaled), supporting the existence of a 569-cm^{-1} mode in H_2COH. However, Johnson and Hudgens[1] recently reanalyzed (experimentally and theoretically) the vibrational spectrum of H_2COH in the ground and in a 3p Rydberg state. For the electronic ground state, they found that the CH_2 wag and torsion motions are coupled (strongly anharmonic), and the newly calculated fundamental frequency of the $\nu_9(CH_2$ wag) mode of 238 cm^{-1} compares very well with an observed value of 234 ± 5 cm^{-1}. No vibrational level at ∼569 cm^{-1} was found, confirming Jacox's assignment of this peak to the H_2CO-HF complex.

For the planar ground state of H_2COH^+, the major change relative to H_2COH(eq) is observed for the CO, CH_2 (both

TABLE 2: Calculated Harmonic Frequencies (in cm^{-1}) for H_2COH and H_2COH^+ [a]

	OH	CH a	CH s	CH_2 s	COH	CO	CH_2 a	CH_2 w	torsion
H_2COH(eq)[b] ^2A C_1									
TW	3928	3331	3180	1529	1399	1237	1090	726	465
JH	3916	3361	3212	1523	1395	1239	1082	[238][c]	[418][c]
BP	3904	3361	3211	1519	1372	1232	1074	612	438
EXP[d]	3650	[3019]	[2915]	1459	1334	1183	1048	[569][e]	420
H_2COH(i) $^2A''$ $C_s(yz)$									
TW	3937	3402	3247	1532	1396	1247	1069	*544i*	*412*
H_2COH(r) $^2A'$ $C_s(xz)$									
TW	3899	3299	3170	1540	1257	1137	*1190*	600	*543i*
GK	3886	3351	3219	1572	1263	1200	*1131*	635	*527i*
H_2COH^+[f] $^1A'$ $C_s(yz)$									
TW	3650	3313	3161	1516	1130	1699	1406	*1265*	*1067*
JH	3620	3313	3163	1508	1126	1694	1398	*[1175][c]*	*[978][c]*
EXP[g]	3423			1459	1091	1623	1351		*993*
H_2COH^+ $^3A''$ $C_s(xz)$									
TW	3532	2962	2844	1123	954	1272	*1043*	462	*595*

[a] All theoretical data at MP2 level, unscaled. See footnote a, Table 1, for references. Italic frequencies correspond to a″ modes. [b] In same order as in table, the absorption intensities (km/mol) are 61, 17, 26, 11, 25, 104, 50, 55, and 94 (TW). [c] Explicitly calculated using a two-dimensional potential energy surface.[1] [d] Reference 6. [e] Reference 1 confirms that this frequency belongs to H_2CO−HF (see text). [f] As in (*b*): 331, 24, 5, 45, 76, 39, 90, and 118 (TW). [g] Taken from ref 1.

TABLE 3: Electric Dipole Moments (μ), Spin Densities and Fermi Contact Terms of the H_2COH Isomers and the H_2CO^- Anion (MP2(full)/6-311++G(2df,2pd) Data)

property	H_2COH(eq)	H_2COH(i)	H_2COH(r)	H_2CO^- [a]
μ (D)	1.521[b]	1.558	1.270	
spin density				
C	1.198	1.199	1.196	1.086
O	0.305	0.324	0.117	0.571
CO	−0.220	−0.244	−0.100	−0.234
H(O)	−0.004	−0.006	0.058	
H(C)	−0.011, −0.031	−0.005, −0.049	−0.040, −0.040	0.053, 0.053
Fermi contact term[c] (au)				
C	0.228	0.151	0.200	0.183
O	0.058	0.063	0.008	0.159
H(O)	−0.002	−0.003	0.020	
H(C)	−0.017, −0.020	−0.029, −0.029	−0.024, −0.024	−0.009, −0.009

[a] Reference 16 (6-311G(2df,2pd) basis set). [b] Reference 15 reports 1.51 (ROHF) and 1.43 D (MRCISD). [c] UHF level.

asymmetric bending and wag), and torsion modes, which increase on average by ∼400 cm^{-1}. As pointed out in ref 1, in the cation the coupling between the CH_2 wag and torsion modes is less severe than in H_2COH(eq); i.e., the harmonic approximation is valid.

The CH stretching modes of $1^3A''$ (H_2COH^+) are significantly smaller than in the ground state, in line with their differences in bond lengths (Table 1).

(3) Electric Dipole and Spin Density Distributions. Table 3 summarizes the electric dipole moments and spin density distributions as calculated for the H_2COH geometries of Table 1, at the MP2(full)/6-311++G(2df,2pd) level. Fermi contact terms (FCT), related to the amount of s-character contained by the SOMO, are calculated at the UHF level.

The electric dipole moment for H_2COH(eq) of 1.52 D is ∼0.7 D smaller than in H_2CO (μ = 2.33 D, experimental[27]). A comparable value of 1.43 D (MR−CISD) was reported earlier.[15] The values calculated at both saddle points are not too different from those at the equilibrium geometry. The dipole moment component along the CO bond is relative small (e.g., 0.31 D for H_2COH(i) and 0.52 D for H_2COH(r)); that is, the total dipole moment is mainly governed by the OH bond.

The calculations clearly show that the spin density is essentially localized at the C center, with that on O being about 7 times smaller. The negative spin density along the CO bond reflects the antibonding character of the π^* SOMO.

According to the FCT data, the hyperfine spectrum of H_2COH is dominated by the C-center. Due to the formation of the OH bond, both the FCT and spin density at the O-center of H_2COH are noticeably smaller than in the isoelectronic H_2CO^- radical (Table 3).

Molecular Orbitals and Ionization Potentials

(1) Canonical Orbital Energies (Ground-State MOs). Table 4 collects the ROHF canonical orbitals energies (valence and 3s,3p Rydberg MOs) of H_2COH at three different conformations, using basis set A. Values for H_2CO are given for comparison. These data allow us to gain some insight into the variations in MO stabilities with changes in geometry, information that is valuable to rationalize trends in ionization potentials, excitation energies, and *g* factors as well.

In this work, the valence MOs are loosely labeled as σ, π, n, and π^*, as customarily done for the $5a_1$, $1b_1$, $2b_2$, and $2b_1$ MOs of H_2CO, respectively (the $1b_2$ species is here called n′). Due to the lower symmetry in H_2COH, however, mixing between MOs is possible, e.g., n/π for the inversion, σ/π for the rotation, and σ/π/n for the equilibrium conformation.

In passing from H_2CO to H_2COH(i), the ordering of the doubly occupied MOs remains unchanged. The n MO (mainly $2p_y$(O)), however, becomes stabilized by ∼2.4 eV, due to mixing of $2p_y$(O) with 1s(H).

For H_2COH(r), the MOs of σ, π, and π^* character are more stable than in H_2COH(i). Quite remarkable is the small energy gap n−π^*, i.e., 2.50 vs 5.55 eV at the inversion geometry or vs 4.57 eV for H_2COH(eq). On the other hand, the energy

TABLE 4: Ground-State Canonical Orbital Energies (in au) of H_2CO and H_2COH (Basis Set A)[a]

H_2CO		H_2COH(eq)		H_2COH(i)		H_2COH(r)	
$3a_1$	−1.4064	3a	−1.3903	3a′	−1.3907	3a′	−1.3815
$4a_1$	−0.8664	4a	−0.8883	4a′	−0.8869	4a′	−0.8870
$1b_2$ (n′)	−0.6916	5a (n′)	−0.7127	5a′ (n′)	−0.7169	5a′ (σ)	−0.6806
$5a_1$ (σ)	−0.6527	6a (σ)	−0.6210	6a′ (σ)	−0.6235	1a″ (n′)	−0.6439
$1b_1$ (π)	−0.5367	7a (π)	−0.5610	1a″ (π)	−0.5564	6a′ (π)	−0.5948
$2b_2$ (n)	−0.4420	8a (n)	−0.5185	7a′ (n)	−0.5293	2a″ (n)	−0.4663
		9a (π*)	−0.3506	2a″ (π*)	−0.3253	7a′ (π*)	−0.3742
$6a_1$ (3s)	0.0559	10a (3s)	−0.1342	8a′ (3s)	0.0577	8a′ (3s)	−0.1348
$2b_1$ ($3p_x$)	0.0593	11a ($3p_x$)	−0.1121	3a″ ($3p_x$)	−0.0836	9a′ ($3p_x$)	−0.1125
$3b_2$ ($3p_y$)	0.0646	12a ($3p_y$)	−0.0932	9a′ ($3p_y$)	0.0657	3a″ ($3p_y$)	0.0676
$7a_1$ ($3p_z$)	0.0917	13a ($3p_z$)	−0.0849	10a′ ($3p_z$)	0.0893	10a′ ($3p_z$)	−0.0847

[a] For H_2COH, the SOMO corresponds to π^*; its MO energy here corroborates that given in ref 4 (∼−0.34 au) but not that in ref 31 (∼−0.10 au). All Rydberg MOs are virtual.

TABLE 5: Vertical Ionization Potentials of H_2COH at Different Conformations (MRD-CI Values, in eV)

MO ionized	H_2COH (eq)		H_2COH (inv)		H_2COH (rot)	
	IP[a]	ΔE[b]	IP	ΔE[b]	IP	ΔE[b]
π*	7.89[c,d]	0.00 (X^1A')	7.47	0.00 (X^1A')	8.73	0.00 (X^1A')
n	12.91[e]	5.02 (1^3A)	13.18	5.71 ($1^3A''$)	11.30	2.57 ($1^3A''$)
	13.54	5.65 (2^1A)	13.64	6.17 ($1^1A''$)	11.43	2.70 ($1^1A''$)
π	13.56	5.67 (2^3A)	13.01	5.54 ($1^3A'$)	14.47	5.74 ($1^3A'$)
	15.68	7.79 (3^1A)	15.54	8.07 ($2^1A'$)	15.85	7.12 ($2^1A'$)
σ	15.64	7.75 (3^3A)	15.52	8.05 ($2^3A''$	17.25	8.52 ($2^3A'$)
	16.27	8.38 (4^1A)	16.21	8.74 ($2^1A''$)	18.25	9.52 ($3^1A'$)
n′	17.82	9.93 (4^3A)	17.83	10.36 ($3^3A''$)	15.95	7.22 ($2^3A''$)
	18.45	10.56 (5^1A)	18.41	10.94 ($3^1A''$)	16.72	7.99 ($2^1A''$)

[a] For comparison, the experimental IPs (vertical, in eV) of H_2CO are 10.88 (n), 14.10 (π), 15.85 (σ), and 16.25 (n′).[27] [b] Vertical transition energies of H_2COH^+ for excitations from n, π, σ and n′ into π*. [c] Adiabatic IP (MRD-CI) = 7.34 eV (7.20 eV, without zero point corrections). Experimental: 8.14 (vert) and 7.56 eV (adiab),[9] and 7.54 eV (adiab).[10] [d] MP2/6-311G(d,p) data: 7.80 (vert) and 7.05 eV (adiab). [e] As in (*d*): 12.86 and 11.56 eV.

separation $\sigma-\pi$* is much higher than for n−π*, but it does not change too much among the H_2COH conformations (e.g., from 7.36 to 8.11 to 8.34 eV in Table 4, from left to right).

In general terms, at the equilibrium geometry the MO's energies lie close to those of the inversion isomer.

In the C_1 conformation, the lowest-lying Rydberg MOs are found to have negative canonical energies; i.e., they contain some σ* valence character, in particular σ^*_{CO} for 3s and $3p_z$. This feature is corroborated by values of the Coulomb integrals J_{ii} around 0.17 au, which are somewhat larger than expected for pure $n = 3$ Rydberg MOs ($J_{ii} \approx 0.1$ au). As well, the total second moment $\langle r^2 \rangle$ reported by Rettrup et al.[15] clearly demonstrates the differences in spatial distributions (in au and relative to the ECC of each MO), namely, 4.5 for π*, 32.0 for 3s, 38.0 for $3p_z$, 54.2 for $3p_y$, and 67.6 for $3p_x$. Rydberg valence mixing, leading to more compact charge distributions, is clearly seen for the 3s and $3p_z$ MOs.

(2) Ionization Potentials. Experimentally, only the vertical and adiabatic values of the first ionization potential (IP) $\pi^* \rightarrow \infty$ have been measured for H_2COH.[9,10] To fill the gap, we have calculated several IPs at three conformations. Table 5 summarizes the IPs predicted at the MRD-CI level, using the ground-state MOs of the neutral radical and basis set A; experimental data for H_2CO are given in footnote *a*.

Using a zero-point energy (ZPE) correction of 0.14 eV[1], a calculated MRD-CI value of 7.34 eV for the first adiabatic IP of H_2COH(eq) is to be compared with experimental values of 7.56 ± 0.01 [9] and 7.540 ± 0.006 eV.[10] The MP2 results (Table 5, footnote *d*) are somewhat smaller than the MRD-CI data, in particular for the adiabatic IP. Using the Gaussian-2 (G2) approximation, adiabatic IP values of 7.36 [28] and 7.45 eV[29] have been reported (both data including ZPE corrections). As seen in Table 5, the H_2COH(i) isomer has the lowest vertical IP $\pi^* \rightarrow \infty$, whereas H_2COH(r) has the largest.

The fact that the first adiabatic IP is ∼0.60 eV smaller than the vertical value implies that ejection of a π* electron is accompained by a significant change in geometry. As shown under Equilibrium Geometries, the ground state of H_2COH^+ has a planar structure similar to H_2COH(i) but with a shorter R(CO) distance. In fact, the experimental photoionization spectrum mainly consists of vibrational progressions in both the CO-stretch and CH_2-wagging motions.[9] The observed $\pi^* \rightarrow$ Ryd spectra show a similar structure.[1,7]

Ionization from the doubly occupied MOs leads to triplet and singlet states of H_2COH^+. Taking the IP into the ground state of the cation as reference, the difference in IPs represents vertical excitation energies of the cation *at the fixed conformation* of H_2COH. In general, ionization from π and σ occurs at energies close to those of H_2CO, whereas the energies for n′ and n (both b_2 MOs in H_2CO) are shifted higher by ∼1 eV.

At the H_2COH(eq) geometry, ionization n $\rightarrow \infty$ takes place at 12.91 eV for 1^3A and at 13.54 eV for 2^1A, to be compared with 10.88 eV for H_2CO (experimental, Table 5). Since the excited state $1^3A''$ of H_2COH^+ has an equilibrium geometry comparable to H_2COH(r) (Table 1), it is understandable why IP (n $\rightarrow \infty$) is the smallest for the rotation conformation. The MP2 value for the vertical IP into 1^3A lies close to the MRD-CI result (Table 5, footnote *e*).

On average, ionization from π occurs at 13.5 eV for the triplet and at 15.5 eV for the singlet state. Such a large triplet−singlet separation is in line with the large value of the exchange integral involving two valence MOs (π and π*) with similar spatial distributions.

Electronic Spectrum

Table 6 summarizes the relative energies of the 3s,3p Rydberg and valence states of H_2COH at different geometries, as obtained at the MRD-CI level with basis set A. Selected values calculated at the equilibrium geometry of the ground state of H_2COH^+, labeled H_2COH(ion), are also included. All data are relative to the H_2COH(eq) minimum of C_1 symmetry.

The MRD-CI relative energies for the ground state at the inversion and rotation conformations are essentially the same as obtained at the MP2 level.

(1) Rydberg States. $\pi^* \rightarrow$ Ryd. The low-energy part of the vertical spectrum of H_2COH(eq), extending from 4.12 to 5.82 eV, is dominated by the 3s and 3p Rydberg states. Using a calculated vertical IP of 7.89 eV, the predicted term values (TV) in electronvolts are 3.77 for 3s, 2.84 for $3p_z$, 2.29 for $3p_y$,

TABLE 6: Excitation Energies of H_2COH at Different Conformations (MRD-CI Values (in eV) Relative to the C_1 Minimum (−114.823 01 au) Basis Set A)

excitation	H_2COH (eq)[a] C_1		H_2COH (inv) $C_s(yz)$	H_2COH (rot)	H_2COH (ion) $C_s(yz)$
GS	0.00 (X^2A)	0.00	0.03 (X^2A'')	0.20 (X^2A') (0.26)[b]	0.45 (X^2A'')
$\pi^* \rightarrow 3s$	4.12 (2^2A)	4.30[c]	3.53 ($1^2A'$)	5.49 ($2^2A'$)	3.23 ($1^2A'$)
$\pi^* \rightarrow 3p_z$	5.05 (3^2A)	5.09[c]	4.43 ($2^2A'$)	6.00 ($3^2A'$)	4.09 ($2^2A'$) [4.34][d]
$\pi^* \rightarrow 3p_y$	5.60 (4^2A)	5.58[c]	5.11 ($3^2A'$)	6.39 ($1^2A''$)	5.04 ($3^2A'$)
$\pi^* \rightarrow 3p_x$	5.82 (5^2A)	5.65[c]	5.37 ($2^2A''$)	6.83 ($4^2A'$)	5.06 ($2^2A''$) [5.09][d]
$n \rightarrow \pi^*$	6.46 (6^2A)	6.70[b]	7.15 ($4^2A'$)	4.97 ($2^2A''$) (5.02)[b]	
$\pi \rightarrow \pi^*$	7.30 (7^2A)	7.77[b]	7.48 ($3^2A''$)	8.27 ($5^2A'$) (8.19)[b]	7.61 ($4^2A'$)
$\sigma \rightarrow \pi^*$	8.40 (8^2A)	9.36[b]	9.91 ($5^2A'$)	10.77 ($6^2A'$)	
$n' \rightarrow \pi^*$				9.59 ($3^2A''$) (9.41)[b]	

[a] Calculated *f*-values: 0.0085 (3s), 0.0100 ($3p_z$), 0.0026 ($3p_y$), 0.0130 ($3p_x$), 0.0039 ($n \rightarrow \pi^*$), 0.0662 ($\pi \rightarrow \pi^*$), and 0.0024 ($\sigma \rightarrow \pi^*$). [b] Theoretical data from ref 31. [c] Theoretical data from ref 15. *f* values: 0.0109 (3s), 0.0171 ($3p_z$), 0.0029 ($3p_y$), and 0.0164 ($3p_x$). [d] Experimental T_0 values.[1,7,8]

and 2.07 for $3p_x$, to be compared with experimental data of 3.79, 2.90, 2.75, and 2.51 eV, respectively, for H_2CO.[30] While the TVs for 3s and $3p_z$ are rather close to the experimental values of H_2CO, those for $3p_y$ and $3p_x$ are ∼0.45 eV smaller in H_2-COH(eq). In any case, the ordering of the 3p states is the same.

The MRD-CI vertical energies for the 3s and 3p states agree, within 0.20 eV, with the values predicted by Rettrup et al.[15] In Table 6, their results have been adapted to our system of coordinates (i.e., exchange between $3p_x$ and $3p_z$).

The calculated oscillator strengths (footnote *a*, Table 6) indicate that the 3s, $3p_z$, and $3p_x$ transitions have similar intensities (*f* values from 0.0085 to 0.0130). The $\pi^* \rightarrow 3p_y$ excitation is somewhat weaker ($f \approx 0.003$), in line with the fact that in C_{2v} symmetry the related transition $\pi^* \rightarrow 3p_y$ ($b_1 \rightarrow b_2$) is dipole forbidden. As shown in footnote *c*, Table 6, Rettrup et al.[15] obtained *f* values similar to ours.

At the geometry of the inversion isomer, the energy of the ground state increases by 0.03 eV, whereas for the $\pi^* \rightarrow$ Ryd states it decreases significantly (on average, by ∼0.5 eV). The reason for this stabilization is simple: the $\pi^* \rightarrow$ Ryd states are expected to have equilibrium geometries similar to that of the $H_2COH^+(^1A')$ core, which in turn is structurally close to H_2-COH(i) (Table 1).

At the H_2COH(r) conformation, the ground-state destabilizes by 0.20 eV, whereas the Rydberg states are shifted to higher energies (on average, by ∼1.0 eV). This finding agrees with the large rotational barrier of the H_2COH^+ core reported by Ha.[4]

Among the geometries studied, the $\pi^* \rightarrow$ Ryd states have the lowest energies at the H_2COH^+(eq) conformation, as expected. The transition energies for the 3s and $3p_z$ states amount to 3.23 and 4.09 eV, respectively, which should be close to the adiabatic values. Relative to a calculated adiabatic IP of 7.20 eV, the corresponding term values are 3.97 and 3.11 eV, i.e., ∼0.20 eV larger than in the vertical region.

Combining an experimental vertical IP(H_2COH) of 8.14 eV with the TVs for the 3d, 4s, and 4p states of H_2CO (2.0, 1.62, and 1.27 eV, from ref 30), the $\pi^* \rightarrow$ 3d, 4s, 4p states of H_2-COH(eq) are expected near 6.1, 6.5, and 6.9 eV, respectively (the corresponding T_0 values should be ∼0.60 eV smaller). In the vertical region, $\pi^* \rightarrow$ 4s thus lies rather close to the $n \rightarrow \pi^*$ state, placed at 6.46 eV (Table 6).

$n \rightarrow$ Ryd. It is of interest to speculate about the location of the Rydberg series of H_2COH(eq) converging to the $n\pi^*$ states $1^3A''$ and $2^1A''$ of H_2COH^+, i.e., the ionization limits $n \rightarrow \infty$.

For H_2COH(eq), as shown in Table 5, IP($n \rightarrow \infty$) lies at 12.91 (1^3A) and 13.54 eV (2^1A). Taking TV(3s) = 3.77 eV as reference, the $n \rightarrow$ 3s ($^{4,2}A$, $n\pi^*3s$) states converging to 1^3A are expected at ∼9.15 eV, i.e., ∼1 eV above the first ionization limit. The same picture holds at the inversion geometry. Since the energy difference between the vertical and adiabatic IP $n \rightarrow \infty$ (triplet state) is ∼1.30 eV (MP2 data, Table 5), the $n \rightarrow$ Ryd spectrum should exhibit a complex vibronic structure.

At the H_2COH(r) conformation, however, $n \rightarrow$ 3s should lie near 7.7 eV or, equivalently, ∼1.2 eV below ground-state H_2-COH^+. Since $H_2COH^+(^3n\pi^*)$ at equilibrium is only 0.14 eV more stable than at the rotation geometry (MP2/6-311G(d,p) results), the band head of the $n \rightarrow$ 3s state should be located close by that energy.

(2) Valence States. To date, no valence transitions have been detected experimentally.

The MRD-CI data in Table 6 show that in most cases the stability of the valence states changes substantially between different H_2COH isomers, as also found in a prior CIPSI study[31] carried out with a valence-only basis set. However, the valence states invariably appear in the order $n \rightarrow \pi^* < \pi \rightarrow \pi^* < \sigma \rightarrow \pi^*$, as in the CIPSI calculations (Table 6); the MRD-CI transition energies for H_2COH(eq), however, are somewhat smaller (by 1 eV for $\sigma \rightarrow \pi^*$).

The $n \rightarrow \pi^*$ excitation of H_2COH(eq), vertically at 6.46 eV, lies ∼3.0 eV higher than in H_2CO,[26,30] reflecting the stabilization of the n MO in the radical (see Molecular Orbitals and Ionization Potentials). At the rotation conformation, however, this state lies at 4.97 eV, the only case in Table 6 where a valence state is more stable than $\pi^* \rightarrow$ 3s. As usual for $n \rightarrow \pi^*$ bands, the absorption intensity is relatively low ($f = 0.0039$).

The $\pi \rightarrow \pi^*$ transition, at 7.30 eV for H_2COH(eq) and having a large *f* value of 0.0662, is a good candidate for studying the valence spectrum experimentally. At the inversion geometry, the $\pi \rightarrow \pi^*$ state at 7.48 eV lies close to the ground state of H_2COH^+ (7.50 eV).

At the equilibrium geometry of H_2COH, $\sigma \rightarrow \pi^*$ is placed at 8.40 eV, ∼0.5 eV higher than the first IP. This state destabilizes drastically in passing to the inversion or rotation conformations, always remaining well above the ground state of H_2COH^+.

In summary, the valence states $\pi \rightarrow \pi^*$ and $\sigma \rightarrow \pi^*$ are more stable at the H_2COH(eq) conformation, whereas $n \rightarrow \pi^*$ and $n' \rightarrow \pi^*$ stabilize at the rotation geometry. On the other hand, all $\pi^* \rightarrow$ Ryd states are more stable at the inversion conformation.

Using the CIPSI method and a valence-only basis set, Solgadi and Flament (SF)[31] studied the dissociation of H_2COH (in the ground and low-lying excited states) into $CH_2 + OH$ and H_2-$CO + H$ as well as the intramolecular arrangement into H_3CO (methoxy radical). They suggested that the failure in detecting fluorescence in the electronic spectrum of H_2COH could be explained by the existence of a very low barrier (<5.5 kcal/mol) in their calculated first excited (valence) state toward the ground state of H_3CO.

Our calculations on the vertical electronic spectrum of H_2-COH(eq), however, cast some doubt on such an explanation.

In detail, Solgadi and Flament placed the lowest-lying state 9a → 10a (from π^* possibly into a σ^* MO) at 6.25 eV, slightly below the n → π^* excitation (Table 6). It is likely that their 9a → 10a excitation tries to mimic a Rydberg transition. If such a valence $\pi^* \rightarrow \sigma^*$ state were in that energy region it would be embedded in the $\pi^* \rightarrow n = 4$ Rydberg manifold (see $\pi \rightarrow$ Ryd), with the consequent existence of numerous vibronic interactions. In fact, detection of n → π^* will also be affected by the same difficulties, in addition to its low *f* value.

(3) Reassignment of the Experimental Spectrum. The ultraviolet absorption spectrum of gaseous H_2COH and its isotopomer D_2COD, extending from 4.3 to 6.0 eV, has been measured by Pagsberg et al.[7] and assigned to $\pi^* \rightarrow$ Ryd transitions. The observed adiabatic excitation energies, with their assignment according to previous ab initio calculations,[15] are (in eV) 4.34 (3s), 5.09 ($3p_z$), 5.58 ($3p_y$), and 5.65 ($3p_x$). The assignment of the last two bands was somewhat uncertain. The transition at $T_0 = 5.09$ eV was also observed in REMPI experiments (refs 1 and 8 and references therein), and there assigned to an unidentified 3p component. All Rydberg bands show a complex vibronic structure, similar to that observed in the PES spectrum (i.e., with progressions in the CO stretch and CH_2 scissor modes dominating).

Rettrup et al.[15] assigned the two lowest (adiabatic) T_0 values at 4.34 and 5.09 eV to $\pi^* \rightarrow 3s$ and $\pi^* \rightarrow 3p_z$, respectively, on the basis of their calculated *vertical* ΔE's of 4.30 and 5.09 eV. However, one has to realize that the corresponding calculated *adiabatic* T_0 values should be ∼0.6 eV smaller, i.e., near 3.7 and 4.5 eV, as inferred from the photoelectron spectrum.[9]

According to ref 1, the zero-point energy of ground-state H_2COH^+ is ∼0.14 eV larger than that of H_2COH(eq), so that experimental T_0's given above correspond to T_e's of approximately 4.20, 4.95, 5.44, and 5.51 eV.

At the H_2COH^+ geometry, our MRD-CI calculations give ΔE values (expected to be close to the T_e's) of 3.23 (3s), 4.09 ($3p_z$), 5.04 ($3p_y$), and 5.06 eV ($3p_x$), to be compared with experimental T_e's of 4.20 and 4.95 eV. Thus, the $\pi^* \rightarrow 3s$ minimum lies ∼1 eV lower than currently assumed in the literature.

A better assignment for the $T_e = 4.20$ eV band is $\pi^* \rightarrow 3p_z$ ($T_e = 4.09$ eV, this work), whereas $T_e = 4.95$ eV is reassigned to $\pi^* \rightarrow 3p_x$ (5.06 eV, this work). The $\pi^* \rightarrow 3p_y$ transition (calculated at 5.04 eV) can be discarded as a possible candidate for the 4.95 eV band because of its low intensity (Table 6).

The experimental peaks at 5.58 and 5.65 eV have previously been assigned to the $3p_y$ and $3p_x$ states,[7] although the possibility for both of them to belong to the $3p_x$ vibrational progression was not ruled out. As shown above, our MRD-CI calculations place the 3p Rydberg states at lower energies. If both peaks are in fact two independent electronic transitions, they could correspond to the $\pi^* \rightarrow$ 3d states, which are expected to have T_0 values near 5.5 eV. Since both $\pi^* \rightarrow 3s$ and $\pi^* \rightarrow 3p_z$ have mixed Rydberg valence character, their quantum defects are expected to be larger than normally found for 3s and 3p Rydberg states.

The spectrum shown in ref 7 gives some indication of an underlying continuum above 5 eV. We suspect that the bond rupture $H_2COH \rightarrow CH_2 + OH$ (all radicals in the ground state), with a dissociation energy near 4.5 eV,[31] is responsible for such a continuum.

Electron-Spin Magnetic Moment

The electron spin magnetic moments (commonly described in terms of *g* factors) for H_2COH have been calculated using basis set A and the GSTEPS suite of programs which has recently been applied to study several small radicals.[16,23,32,33] ROHF calculations were performed on all isomers, whereas MRD-CI results are available for the rotation and C_{2v} structures only (see Tables 7−9). In all cases, the electronic charge centroid serves as the origin of coordinates.

TABLE 7: Calculated Diagonal *g* Shifts for Different Conformations of H_2COH (ROHF Data (in ppm), Basis Set A)[a]

		Δg_{xx}		Δg_{yy}		Δg_{zz}		
species	Δg_{RMC}	1st	2nd	1st	2nd	1st	2nd	Δg_{av}[b,c]
equil	−154	−64	22	−14	1178	1	708	456
inversion	−152	−75	−3	−18	1344	1	867	553
rotation	−143	−70	34	−23	576	−2	751	279
C_{2v}	−153	−75	−4	−19	968	3	1093	502

[a] $\Delta g_{ii}^{total} = \Delta g_{RMC} + \Delta g_{ii}(1st) + \Delta g_{ii}(2nd)$. [b] $\Delta g_{av} = {}^1/_3(\Delta g_{xx}^{tot} + \Delta g_{yy}^{tot} + \Delta g_{zz}^{tot})$. [c] Using basis set B, Δg_{av} is 557, 273, and 509 ppm for the inversion, rotation, and C_{2v} conformations, respectively.

Let us first consider the C_{2v} system, for which the Δg tensor is diagonal (only Δg_{xx}, Δg_{yy}, and Δg_{zz} are nonzero). Each component is essentially governed by the magnetic coupling with just one excited state. At lower symmetries, however, an excited state might contribute to several Δg components, including nondiagonal terms. The ground state of $H_2COH(C_{2v})$, $^2B_1(1b_2^2 5a_1^2 1b_1^2 2b_2^2 2b_1$, or $\sigma^2\pi^2 n^2 \pi^*)$, is magnetically coupled with excited states of type $^2A_2(x)$, $^2A_1(y)$, and $^2B_2(z)$. The second-order contribution to Δg_{xx} is practically zero (−4 ppm) since there are no valence MOs of a_2 character. For Δg_{yy}, relevant coupled $^2A_1$ states include $5a_1 \rightarrow 2b_1$ ($\sigma \rightarrow \pi^*$) and $2b_1 \rightarrow 6a_1$ ($\pi^* \rightarrow \sigma^*$), with positive and negative contributions, respectively. The main excitations for Δg_{zz} comprise n → π^* and n′ → π^*, with the former predominating because of its lower excitation energy. As seen in Table 7, second-order contributions to Δg_{yy} and Δg_{zz} lie around 1000 ppm each. Combined with the first-order terms, this leads to a Δg_{av} value of ∼500 ppm.

For the other conformations, the Δg_{RMC} term remains essentially the same as for the C_{2v} isomer (∼−150 ppm). The Δg_{xx} component also remains very small, a feature that can be traced to the situation prevailing at the C_{2v} symmetry.

For H_2COH, both at the equilibrium and inversion conformations, Δg_{yy} is larger than Δg_{zz}, by ∼470 ppm. The total Δg_{yy} value of the inversion geometry is ∼150 ppm larger than that at equilibrium. The results in Table 7 indicate that Δg_{av} lies in the 500 ± 50 ppm region (i.e., close to the C_{2v} value). Since both conformations are essentially isoenergetic, the vibrational average of the ROHF Δg data will also give ∼500 ± 50 ppm for Δg_{av}. On the other hand, for the less stable rotation geometry, Δg_{av} is ∼220 ppm smaller, mainly because of a significant decrease in the Δg_{yy} contribution.

The ROHF Δg values obtained with basis set B (Table 7, footnote *c*) are essentially the same as those with basis set A.

For planar H_2COH(i) with $C_s(yz)$ symmetry, the ground state is $X^2A''(7a'^2\ 2a'')$. The correlation $C_s(yz) - C_{2v}$ is $^2A' \rightarrow (^2A_1, ^2B_2)$ and $^2A'' \rightarrow (^2A_2, ^2B_1)$. That is, X^2A'' couples with excited states of type $^2A''(x)$ and $^2A'(y,z)$. Here, the $\Delta\mathbf{g}$ tensor is diagonal only in Δg_{xx} (component perpendicular to the molecular plane). The main valence excited state of $^2A''$ symmetry is $\pi \rightarrow \pi^*$, whereas valence states of $^2A'$ character include excitations from n′, σ, or n into π^*.

For H_2COH(r) with $C_s(xz)$ symmetry, the ground state is $X^2A'(2a''^2 7a')$. The correlation $C_s(xz) - C_{2v}$ is $^2A' \rightarrow (^2A_1, ^2B_1)$ and $^2A'' \rightarrow (^2A_2, ^2B_2)$. Here, X^2A' is magnetically coupled with excited states of type $^2A''(y)$ and $^2A'(x,z)$. The Δg-tensor

TABLE 8: Second-Order Contributions to the Diagonal *g* Shifts of H_2COH at Different Geometries (ROHF Data (in ppm), Basis set A)

	equil			inver			rot		
excitation	Δg_{xx}	Δg_{yy}	Δg_{zz}	Δg_{xx}	Δg_{yy}	Δg_{zz}	Δg_{xx}	Δg_{yy}	Δg_{zz}
n′ → π*	4	207	−73	0	235	−82	−12	0	71
σ → π*	34	858	28	0	964	48	0	498	0
π → π*	2	−3	100	0	0	0	0	349	0
n → π*	11	177	874	0	166	1060	65	0	807
π* → 3s[a]	5	−197	−2	0	−104	−2	0	−184	0
sum (5 states)	56	1042	927	0	1261	1024	53	663	878
rest	−34	136	−119	0	83	−157	−19	−87	−127
total (2nd)	22	1178	708	−3	1344	867	34	576	751
total(1st + 2nd)[b]	−196	1010	555	−230	1174	716	−179	411	606

[a] The 3s MO has some σ^*_{CO} contribution. [b] See Table 7 for first-order terms.

TABLE 9: Comparison of ROHF and MRDCI Data for Relevant Excited States of H_2COH. Basis Set A

	SO (cm^{-1})	*L* (au)		ΔE (eV)		Δg(ppm)	
	ROHF[a]	ROHF	MRDCI	ROHF	MRDCI	ROHF	MRDCI[b]
σ → π*							
equil							
y	23.44	0.8048	0.6072	10.90	8.40	858	840
z	1.52	0.4009	0.6815			28	62
x	3.46	0.2165	0.1700			34	35
inv							
y	24.64	0.8569	0.8723	10.86	9.91	964	1075
z	2.32	0.4543	0.3561			48	41
rot							
y	17.69 [15.43]	0.7433	0.6593	13.09	10.77	498	537 [468]
C_{2v}[c]							
y	24.38 [13.30]	1.1349	0.4009	13.03	11.01	1056	441 [241]
	[18.28]		1.2747		11.93		[972]
n → π*							
equil							
z	21.18	0.7368	0.7726	8.85	6.46	874	1256
y	11.34	0.2790	0.2956			177	257
x	2.51	0.0789	0.0430			11	8
inv							
z	23.38	0.8218	0.8527	8.99	7.15	1060	1383
y	10.59	0.2841	0.2941			166	216
rot							
z	19.21	0.6398	0.6701	7.55	4.97	807	1284
x	8.05	0.1222	0.1095			65	88
C_{2v}							
z	28.04 [28.84]	0.7148	0.7689	7.69	5.58	1296	1922 [1977]
π → π*[d]							
equil							
x	1.53	0.0509	0.0578	10.82	7.30	2	2
y	1.85	0.0355	0.0204			−3	−6
z	7.13	0.3068	0.0423			100	20
inv							
x	0.01	0.0056	0.0359	10.83	7.48	0	0
rot							
y	12.26 [12.25]	0.6393	0.6808	11.12	8.27	349	500 [500]

[a] MRD-CI values in brackets. [b] Using MRDCI values for *L* and ΔE but ROHF for SO. [c] This excitation contributes by 41 and 38% to two $^2A_1$ states; the interacting excitation is π* → σ* (46 and 47%, respectively). [d] This excitation does not contribute at all to Δg of the C_{2v} conformation.

is diagonal only in Δg_{yy} (component perpendicular to the symmetry plane). Relevant excited states include σ → π*, π → π*, and π* → 3s for $^2A'$, and n → π* for the $^2A''$ symmetry.

The second-order contributions to the ROHF *g* shifts of H_2COH due to five selected excitations are displayed in Table 8. At the equilibrium geometry, the Δg_{zz} component (parallel to the CO bond) is governed by the n → π* coupling (874 ppm), whereas the contributions from n′ → p* and π → π* nearly cancel each other. The total second-order contribution is 708 ppm.

The n → π* excitation also dominates Δg_{zz} at the inversion (1060 ppm) and rotation (807 ppm) geometries. The corresponding total second-order contributions to Δg_{zz} are about 150 and 50 ppm higher than for H_2COH(eq).

For both the equilibrium and inversion geometries, σ → π* constitutes the main contributor to Δg_{yy} (∼900 ppm on average). For H_2COH(r), due to the strong σ−π mixing, one has to consider the contributions of σ → π* and π → π* together. The final value, 847 ppm, is similar to that at equililibrium (858 ppm).

The excitation π → π* does not contribute at all to Δg_{av} of the C_{2v} structure (due to symmetry) and very little to the equilibrium and inversion isomers (because of the small values of SO and L). Its apparent contribution to Δg_{yy} of H_2COH(r)

is a consequence of the σ/π mixing. The significant (negative) contribution of the $\pi^* \rightarrow$ 3s state to Δg_{yy} confirms the mixed-valence Rydberg character of the 3s MO.

Table 9 summarizes the values of the spin−orbit (SO) and angular momentum (L) matrix elements and the transition energy ΔE obtained for the excitations $\sigma \rightarrow \pi^*$, n $\rightarrow \pi^*$, and $\pi \rightarrow \pi^*$ of H_2COH at different conformations. The SO matrix elements were calculated at the ROHF level; correlated data are available for $\sigma \rightarrow \pi^*$ of the rotation and C_{2v} structures and for n $\rightarrow \pi^*$ of the C_{2v} conformation.

Using the data of Table 9, it is found that correlation increases the contributions of $\sigma \rightarrow \pi^*$ to Δg_{yy} by ∼110 ppm (∼12%), and that of n $\rightarrow \pi^*$ to Δg_{zz} by ∼320 ppm (∼30%).

The main difference between the ROHF and CI Δg values arises from the excitation energies, which are invariably overestimated at the monodeterminantal level, on average by ∼2.50 eV. Relative to an average $\Delta E \approx 8.15$ eV (MRD-CI), this corresponds to an understimation error for Δg_{av} of ∼30%.

The results above suggest that a full correlated treatment of the SOS expansion would increase the ROHF Δg_{av} values by ∼150 ppm. Thus, including correlation, Δg_{av} is estimated to be 650 ± 50 ppm for both the equilibrium and inversion conformations. This has to be compared with experimental values lying at ∼1000 ppm for H_2COH in solution (see Introduction). Since in condensed media the Rydberg states are known to be supressed,[34] the Δg contribution of ∼−200 ppm resulting from the $\pi^* \rightarrow$ 3s (mixed with σ^*) state of *gaseous* H_2COH(eq) might probably be reduced by half, or so. Altogether, our best estimate for $\Delta g_{av}(H_2COH$, solution) is 750 ± 50 ppm.

Summary and Concluding Remarks

In this work, several properties of H_2COH have been studied theoretically.

The MRD-CI data indicate that the current assignment of the experimental absorption spectrum is probably incorrect. Contrary to earlier assumptions in the literature,[7,15] the Rydberg transition $\pi^* \rightarrow 3p_z$, rather than $\pi^* \rightarrow$ 3s, is responsible for an absorption band at $T_0 = 4.34$ eV. Similarly, a band head at $T_0 = 5.09$ eV is reassigned to $\pi^* \rightarrow 3p_x$. According to our results, the first transition constitutes a (CO) perpendicular type of band, and the second, a parallel band.

Two peaks observed at 5.58 and 5.65 eV, assuming that they are not components of the vibrational progression of the $3p_x$ state, are difficult to classify. On the basis of experimental data for the IP (adiabatic) of H_2COH and the 3d term value of H_2-CO, both peaks lie close to the energy region expected for the $\pi^* \rightarrow$ 3d states ($T_0 \approx 5.5$ eV).

It is not clear to us why the 3s state (with a *f* value similar to $\pi^* \rightarrow 3p_z$) is not seen in the experimental spectrum. It is possible that regions of low energy (the band head of the 3s state lies below 30 000 cm^{-1}) have not been scanned.[7]

Due to the formation of the OH bond, the n MO of H_2COH is stabilized with respect to H_2CO, resulting in a higher energy for n $\rightarrow \pi^*$. In fact, this excited state is expected to lie close to $\pi^* \rightarrow$ 4s. The $\sigma \rightarrow \pi^*$ state lies within the first ionization continuum. In contrast to H_2CO, where the ^{3,1}(n $\rightarrow \pi^*$) and $^3(\pi \rightarrow \pi^*)$ states are more stable than the Rydberg manifold, for H_2COH both excitations lie either within the $n = 4$ Rydberg states or slightly below the first IP.

The second-order contribution to the g shift of H_2COH is dominated by the magnetic coupling of the ground state with the excited states n $\rightarrow \pi^*$ and $\sigma \rightarrow \pi^*$. Although Rydberg states usually do not contribute to the g shifts, in the case of H_2COH the $\pi^* \rightarrow$ 3s state has a significant contribution of −200 ppm because of the $3s/\sigma^*_{CO}$ Rydberg valence mixing.

The Δg_{av} value of the H_2COH radical is ∼500 ppm smaller than for the isoelectronic H_2CO^- anion. The main reason for this difference lies in the transition energies of the valence states, which are smaller in the anion.[16]

It would of interest to carry out ESR experiments on (gaseous) H_2COH at higher temperatures in order to populate H_2COH(r), since according to our calculations, this process will lead to a decrease of Δg_{av}.

Acknowledgment. Financial support by the Natural Sciences and Engineering Research Council of Canada (NSERC) is gratefully acknowledged. The authors also thank David Lonergan for preparing Figure 1, and one of the reviewers for valuable comments.

References and Notes

(1) Johnson, R. D.; Hudgens, J. W. *J. Chem. Phys.* **1996**, *100*, 19874.
(2) Saebo, S.; Radom, L.; Schaefer, H. F. *J. Chem. Phys.* **1983**, *78*, 845.
(3) Bauschlicher, C. W.; Partridge, H. *Chem. Phys. Lett.* **1993**, *215*, 451; *J. Phys. Chem*. **1994**, *98*, 1826.
(4) Ha, T. *Chem. Phys. Lett.* **1975**, *30*, 379.
(5) Adams, G. F.; Bartlett, R. J.; Purvis, G. D. *Chem. Phys. Lett.* **1982**, *87*, 311.
(6) Jacox, M. E.; Milligan, D. E. *J. Mol. Spectrosc*. **1973**, *47*, 148. Jacox, M. E. *Chem. Phys.* **1981**, *59*, 213.
(7) Pagsberg, P.; Munk, J.; Simpson, V. J. *Chem. Phys. Lett.* **1988**, *146*, 375; *Chem. Phys. Lett.* **1989**, *157*, 271.
(8) Dulcey, C. S.; Hudgens, J. W. *J. Chem. Phys.* **1986**, *84*, 5262.
(9) Dyke, J. M.; Ellis, A. R.; Jonathan, N.; Keddar, N.; Morris, A. *Chem. Phys. Lett.* **1984**, *111*, 207. Dyke, J. M. *J. Chem. Soc., Faraday Trans. 2* **1987**, *83*, 69.
(10) Ruscic, B.; Berkowitz, J. *J. Chem. Phys.* **1991**, *95*, 4033.
(11) Zeldes, H.; Livingston, R. *J. Chem. Phys.* **1966**, *45*, 1946.
(12) Krusic, P. J.; Meakin, P.; Jesson, J. P. *J. Phys. Chem.* **1971**, *75*, 3438.
(13) Eiben, K.; Fessenden, R. W. *J. Phys. Chem.* **1971**, *75*, 1186.
(14) Davies, A. G.; Neville, A. G. *J. Chem. Soc., Perkin Trans. 2* **1992**, 163.
(15) Rettrup, S.; Pagsberg, P.; Anastasi, C. *Chem. Phys.* **1988**, *122*, 45.
(16) Bruna, P. J.; Lushington, G. H.; Grein, F. *Chem. Phys.* **1997**, *225*, 1.
(17) Frisch, M. J.; Head-Gordon, M.; Trucks, G. W.; Foresman, J. B.; Schlegel, H. B.; Raghavachari, H.; Robb, M. A.; Binkley, J. S.; Gonzalez, C.; DeFrees, D. F.; Fox, D. F.; Whiteside, R. A.; Seeger, R.; Melius, C. F.; Baker, J.; Martin, R. L.; Kahn, L. R.; Stewart, J. P.; Topiol, S.; Pople, J. A. *GAUSSIAN90*; (Gaussian Inc., Pittsburgh, 1990.
(18) Buenker, R. J.; Peyerimhoff, S. D.; Butscher, W. *Mol. Phys*. **1978**, *35*, 771. Knowles, D. B.; Álvarez-Collado, J. R.; Hirsch, G.; Buenker, R. J. *J. Chem. Phys.* **1990**, *92*, 585, and references therein.
(19) Huzinaga, S. *J. Chem. Phys*. **1965**, *42*, 1293.
(20) Dunning, T. H. *J. Chem. Phys*. **1971**, *55*, 716.
(21) Sadlej, A. J. *Collect. Czech. Chem. Commun*. **1988**, *53*, 1995.
(22) Harriman, J. E. *Theoretical Foundations of Electron Spin Resonance*; Academic Press: New York, 1978.
(23) Lushington, G. H.; Grein, F. *Theor. Chim. Acta* **1996**, *93*, 259; *Int. J. Quantum Chem.* **1996**, *60*, 1679; *J. Chem. Phys.* **1997**, *106*, 3292.
(24) Schreckenbach, G.; Ziegler, T. *J. Phys. Chem. A* **1997**, *101*, 3388.
(25) Glauser, W. A.; Koszykowski, M. L. *J. Phys. Chem*. **1991**, *95*, 10705.
(26) Bruna, P. J.; Hachey, M. R. J.; Grein, F. *J. Phys. Chem.* **1995**, *99*, 16576.
(27) Bruna, P. J.; Hachey, M. R. J.; Grein, F. *J. Mol. Struct. (THEOCHEM)* **1997**, *400*, 177.
(28) Curtiss, L. A.; Kock, L.; Pople, J. A. *J. Chem. Phys.* **1991**, *95*, 4040.
(29) Ma, N. L.; Li, W.-K.; Chong, D. P.; Ng, C. Y. *Chem. Phys.* **1994**, *179*, 365.

(30) Hachey, M. R. J.; Bruna, P. J.; Grein, F. *J. Phys. Chem.* **1995**, *99*, 8050.
(31) Solgadi, D.; Flament, J.-P. *Chem. Phys.* **1985**, *98*, 387.
(32) Lushington, G. H. Ph.D. Thesis, University of New Brunswick, Fredericton, New Brunswick, Canada.
(33) Lushington, G. H.; Bruna, P. J.; Grein, F. *Z. Phys. D* **1996**, *36*, 259; *Int. J. Quantum Chem.* **1997**, *63*, 511. Bruna, P. J.; Lushington, G. H.; Grein, F. *Chem. Phys. Lett.* **1996**, *258*, 427.
(34) Robin, M. B. *Higher Excited States of Polyatomic Molecules*; Academic Press: New York, 1974.